Anal. Chem. **2001,** *73,* 4364−4373

Spike Removal and Denoising of Raman Spectra by Wavelet Transform Methods

F. Ehrentreich* and L. Sümmchen

Technische Universität Dresden, Institut für Analytische Chemie, D-01062 Dresden, Germany

Wavelet decompositions of Raman spectra were investigated with respect to their usability for spike removal and denoising of the raw data. It could be shown that those operations should be performed sequentially. Suppression of spikes is not straightforwardly possible by wavelet transformation; however, the wavelet transform may be used to recognize the spikes by their first level detail coefficients. Spike locations could be projected from the details to the approximations and, further, to appropriate locations of the original spectrum. After spike recognition, those regions will be replaced by interpolated values. To complete processing, denoising is performed with the despiked spectrum by repeated application of wavelet transform methods.

Charge-coupled devices (CCD) are increasingly used in dispersive Raman spectroscopy because of their high-quantum efficiency and their low-dark current.[1] Several noise sources can occur using a CCD detector. The total noise of the system is composed of the shot noise, the dark-current noise, and the readout noise; however, noise is more sample-dependent than detector-dependent. One important cause may be attributed to unspecific absorption of radiation by colored or black samples, resulting in a poor signal-to-noise ratio.

An even more serious problem concerning usage of CCD detectors consists of their sensitivity to cosmic rays, such as muons and other ionizing particles. Such particles provoke a charge up to several thousand electrons to a single element or over a few consecutive elements of the CCD detector. As result of those cosmic ray events, sharp lines exhibiting full width at half of maximum (fwhm) up to 1 cm^{-1}, so-called spikes, are spuriously introduced into Raman spectra.

Noise removal is one of the most important operations of data processing. Despite its widespread use, no general strategy of denoising exists. Selection of denoising strategies, including parameter selection, is strongly problem-dependent. It depends on the signal-to-noise ratio (S/N), the shape of the signals and its superposition, the resolution of complex overlaid signals, and justification or violation of model assumptions regarding noise distribution.

The amplitude of noise at a temporal instant cannot be predicted and the cause of its appearance is unknown. Spikes have in common with noise the first property; however, they differ with regard to the second. A straightforward discrimination could be achieved if its frequency components would be sufficiently high to separate them from those of signals; otherwise, more sophisticated procedures have to be applied.

The recent development of wavelet theory by mathematicians and computer scientists (cf. refs 2−8) has attracted much attention in the applied sciences. Introductions and overviews from a chemometrical point of view have also been published.[9−12] Chemical applications cover fields as denoising, compressing, and variable selection for signals,[13−21] as well as for images.[22,23]

Besides applications in these fields, the wavelet transform has been applied for recognition of signal discontinuities[24,25] or contrast enhancement of edges in image processing.[26]The current work

* Corresponding author. Present address: Universität zu Köln, Institut für Biochemie, Zülpicher Strasse 47, D-50674 Köln, Germany.

(1) Deckert, V.; Kiefer, W. *Appl. Spectrosc.* **1992**, *46*, 322−328.
(2) Daubechies, I. *Ten Lectures on Wavelets*; SIAM: Philadelphia, PA, 1992.
(3) Kaiser, G. *A Friendly Guide to Wavelets*; Birkhäuser: Boston, MA, 1994.
(4) Chui, C. K. *An Introduction to Wavelets*; Academic Press: NewYork, 1992.
(5) Strang, G.; T. Nguyen, T. *Wavelets and Filter Banks*; Wellesley-Cambridge Press: Wellesley, MA, 1996.
(6) Wickerhauser, M. V. *Adapted Wavelet Analysis from Theory to Software Algorithms*; A. K. Peters: Wellesley, MA, 1994.
(7) Stollnitz, E. J.; DeRose, T. D.; Salesin, D. H. *IEEE Comput. Graphics Appl.* **1995**, 76−84.
(8) Stollnitz, E. J.; DeRose, T. D.; Salesin, D. H. *IEEE Comput. Graphics Appl.* **1995**, 75−85.
(9) Walczak, B., Ed. In *Data Handling in Science and Technology*; Elsevier Science: Amsterdam, 2000, Vol. 22.
(10) Walczak, B.; Massart, D. L. *Trends Anal. Chem.* **1997**, *16*, 451−463.
(11) Alsberg, B. K.; Woodward, A. M.; Kell, D. B. *Chemom. Intell. Lab. Syst.* **1997**, *37*, 215−239.
(12) Leung, A. K.-M.; Chau, F.-T.; Gao, J.-B. *Chemom. Intell. Lab. Syst.* **1998**, *43*, 165−184.
(13) Bos, M.; Vrielink, J. A. M. *Chemom. Intell. Lab. Syst.* **1994**, *23*, 115−122.
(14) Barclay, V. J.; Bonner, R. F.; Hamilton. I. P. *Anal. Chem.* **1997**, *69*, 78−90.
(15) Woodward, A. M.; Alsberg, B. K.; Kell, D. B. *Chemom. Intell. Lab. Syst.* **1998**, *40*, 101−107.
(16) Mittermayr, C. R.; Rosenberg, E.; Grasserbauer, M. *Anal. Commun.* **1997**, *34* (2), 73−75.
(17) Mittermayr, C. R.; Nikolov, S. G.; Hutter, H.; Grasserbauer, M. *Chem. Intell. Lab. Syst.* **1996**, *34*, 187−202.
(18) Ehrentreich, F.; Nikolov, S.; Wolkenstein, M.; Hutter, H. *Mikrochim. Acta* **1998**, *128*, 241−250.
(19) Cai, C.; de Harrington, P. *J. Chem. Inf. Comput. Sci.* **1966**, *6*, 1161−1170.
(20) Jouan-Rimbaud, D.; Walczak, B.; Poppi, R. J.; de-Noord, O. E.; Massart, D. L. *Anal. Chem.* **1997**, *69* (21), 4317−4323.
(21) Alsberg, B. K.; Woodward, A. M.; Winson, M. K.; Rowland, J. J.; Kell, D. B. *Anal. Chim. Acta* **1998**, *368*, 29−44.
(22) Nikolov, S. G.; Hutter, H.; Grasserbauer, M. *Chem. Intell. Lab. Syst.* **1996**, *34*, 263−273.
(23) Wolkenstein, M.; Hutter, H.; Nikolov, S. G.; Grasserbauer, M. *Fresenius' J. Anal. Chem.* **1997**, *357*, 783−788.
(24) Mallat, S. G.; Hwang, W.-L. *IEEE Trans. Inf. Theory* **1992**, *38*, 617−643.
(25) Stork, C. L.; Veltkamp, D. J.; Kowalski, B. R. *Appl. Spectrosc.* **1998**, *52*, 1348−1352.
(26) Wolkenstein, M.; Kolber, T.; Nikolov, S.; Hutter, H. J. *Trace Microprobe Technol.* **2000**, *18*, 1−14.

10.1021/ac0013756 CCC: $20.00
Published on Web 07/27/2001

is devoted to investigations for processing Raman spectra by the wavelet transform, because first topic spike removal had to be performed and second denoising was important. In adaptation to the term denoising, we will use the term "despiking" as a synonym for spike removal. In the given context, accuracy is related to correct band recognition. Hence, false positive recognition means that a spike was mistaken as band. Conversely, a false negative conclusion relates to wrong suppression of bands. Obviously, the later problem is more serious.

THEORY

For analyzing, a signal's frequency content signal analysis has the Fourier analysis at its disposal; however, Fourier analysis has the disadvantage of losing time information after transforming a signal into the frequency domain. Hence, it is impossible to indicate when a particular event took place. However, even that information is important when analyzing nonstationary signal features, as drift, discontinuities, or beginnings and ends of signal features.

To cope with these problems, the windowed Fourier transform (WFT or Gabor transform) may be applied. The window truncates the sine and cosine functions to fit a window of a given width. Because a unique window is used for all of the frequencies in the WFT, the resolution of the analysis is the same over the whole domain and is limited by the size of the window.

With wavelet analysis, the window size can be varied. We could say that it delivers a zooming lens for global and local features; hence, the basic advantage over the classical signal processing transformations is its ability to process both time and frequency together. There is a relationship between wavelet scales and frequency. At low scale, compressed wavelets are used. They correspond to fast-changing details, that is, to a high frequency. At high scale, the wavelets are stretched. They correspond to slowly changing features, that is, to a low frequency.

In continuous wavelet analysis, the wavelet coefficients, c, are related to the signal according to

$$c(p,q) = \int_R y(t)\frac{1}{\sqrt{p}}\psi\left(\frac{x-q}{p}\right)\mathrm{d}t \qquad (1)$$

where x and y describe the original signal, p characterizes the scale and resolution and q characterizes the translation.

In discrete wavelet transform (DWT) p and q take discrete values according to

$$p = 2^j, \quad q = k2^j, \quad j \in N, \quad k \in Z$$

With respect to index j, a unique nomenclature does not exist. Some authors will characterize the approximation of the data vector at fine scale by a large index j of scaling functions $\phi_{j,k}$ and wavelets $\psi_{j,k}$, where j denotes the level of decomposition and k denotes the translation. To be in accordance with the software used,[27] we will follow the nomenclature of ref 28. Hence, the data vector at fine scale has a small index, j; that is, the original data are characterized by zero index j. Consequently, as j increases, the resolution 2^{-j} decreases and coarser details will be described.

A real breakthrough regarding applications of the wavelet transform in the applied sciences has only been achieved after Mallat[29,30] had developed efficient algorithms for performing the discrete wavelet transform (DWT) in dyadic scales, sometimes referred to as pyramidal algorithms. Wavelet decomposition may be investigated from the point of view of filter design, because a relationship of wavelets and quadrature mirror filters exists. The wavelet functions ψ are determined by high-pass filters (g) and scaling functions ϕ are related to low-pass filters (h). The signal or approximation coefficients a_j will be hierarchically transformed to approximation (a_{j+1}) and detail coefficients (d_{j+1}) by deconvolution with filters h and g and subsequent downsampling. The original spectrum might be considered as the approximation at level 0 by the a_0 coefficients.

As a generalization, the wavelet packet transform[31−33] enriches the decomposition structure, also permitting the decomposition of the detail coefficients. Conversely, during wavelet synthesis, upsampling and joined convolution of approximation and detail coefficients from level $j + 1$ with the appropriate filters will reconstruct the approximation coefficients at level j. Further, the separate convolution of approximation or detail coefficients, respectively, lead to successive reconstructions of the signal, that is, approximations A_j and details D_j. The resemblance of the signal to approximations A_j is higher as j diminishes. For a more comprehensive introduction to the theory of wavelet transform, the reader should consult the mathematical[2−8] or chemometrical[9−12] literature.

The different decompositions and reconstructions of the signals, Raman spectra in our case, may be performed in a way to exist in the same x-axis grid (cf. Figure 1). In the uppermost two panels, the normalized Raman intensity $I_{\mathrm{normalized}}$ is displayed as a function of the Raman shift. We will denote this relationship in short as $y = f(x)$. Below, wavelet approximations and details from levels 1−4 are represented as functions of the Raman shift. We make use of the fact that an index, i, of detail $D_2(x_i)$, for example, that of an approximation $A_3(x_i)$ and that of the spectrum $y(x_i)$, identify the same instant of observation. This kind of representation enables us to analyze simultaneously both the time and the frequency behavior of a signal.

Similarly to Fourier analysis, the wavelet transform most often consists of three aspects: (i) decomposing a signal to obtain wavelet coefficients in the transformed domain, (ii) analysis and processing of the wavelet coefficients in that domain, and (iii) reconstructing the signal from the modified coefficients. We do so if we have the expectation that the correlation between some properties and the wavelet coefficients is more pronounced as the correlation with the primary features in the original domain.

Recently, the established methods as polynomial smoothing and Fourier filtering procedures were enriched by wavelet applications, initiated by Donoho et al.[34−36] Barclay et al. [14]

(27) Misiti, M.; Misiti, Y.; Oppenheim, G.; Poggi, J.-M. *Wavelet Toolbox*; The Mathworks Inc.: Natick, MA, 1997.

(28) Misiti, M.; Misiti, Y.; Oppenheim, G.; Poggi, J.-M. *Wavelet Toolbox User's Guide*; The Mathworks Inc.: Natick, MA, 1997.

(29) Mallat, S. G. *IEEE Trans. Acoust. Speech Signal Process.* **1989**, *37*, 2091−2110.

(30) Mallat, S. G. *IEEE Trans. PAMI* **1989**, *11*, 674−693.

(31) Coifman, R. R.; Wickerhauser, M. V. *IEEE Trans. Inf. Theory* **1992**, *38*, 713.

(32) Wickerhauser, M. V. In *Proceedings ondelettes et paquets d'ondes*; Rocquencourt: France, 1991; pp 31−99.

(33) Walczak, B.; Massart, D. L. *Chemom. Intell. Lab. Syst.* **1997**, *36*, 81−94.

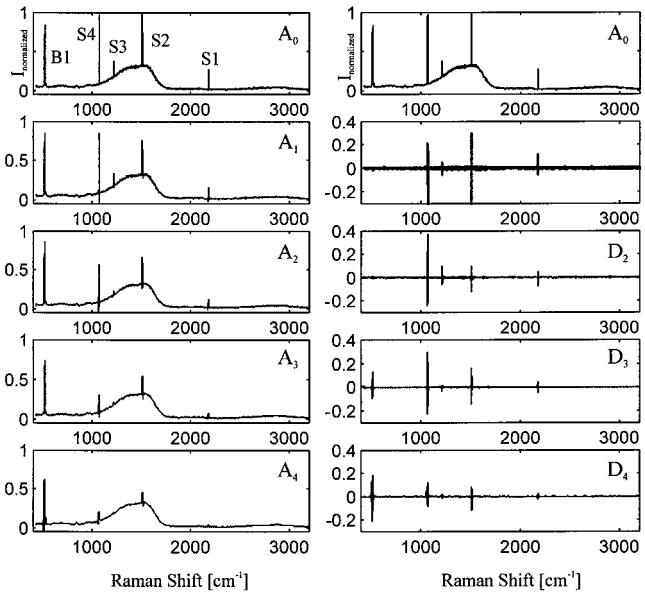

Figure 1. Representation of approximations A_j and details D_j for the Raman spectrum of the carbon nitride film in a unique *x*-axis grid.

performed a careful comparison between established methods and wavelet strategies. They compared Savitzky−Golay smoothing, Fourier filtering, and different wavelet thresholding procedures and applied them to model signals and experimental spectra. They also addressed a crucial problem, threshold selection, and summarized three strategies to estimate suitable thresholds: (i) visual evaluation of the raw vs processed data, (ii) statistical analysis of the noise as the difference between raw and processed data, and (iii) signal and spectrum simulation, including the addition of artificial noise.

For wavelet analysis, the parameter selection depends on the wavelet basis, level of decomposition, threshold type selection, and threshold selection. The widespread use of empirical methods for threshold selection depends on the fact that the noise distribution is often not well-known.

The noisy signal may be described by

$$y(x) = \hat{y}(x) + \sigma e(x) \tag{2}$$

where $e(x)$ is supposed to be Gaussian noise and the detail coefficients of the finest scale d_1 are supposed to be essentially noise coefficients with standard deviations equal to σ. Under these circumstances, the noise level σ could be estimated[37] by

$$\sigma = \text{median}(\text{abs}(d_1))/0.6745 \tag{3}$$

For denoising, in contrast to compression, soft thresholding according to

$$\hat{d}_{j,k} = \text{sign}(\boldsymbol{d}_{j,k})(|d_{j,k}| - \text{thr}) + \tag{4}$$

is generally applied as threshold type.

Supposing Gaussian noise with unit standard deviation, as threshold thr, the fixed-form threshold equal to $\sqrt{2 \log n}$ has been applied. To check whether nonwhite noise has to be supposed, a level-dependent estimation of the thresholds has been applied according to

$$\text{thr}_{\text{level}} = \sigma_{\text{level}}\sqrt{2 \log n} \tag{5}$$

EXPERIMENTAL SECTION

The Raman measurements were performed using the microscope of a dispersive Raman spectrometer Dilor XY 800 (DILOR SA, Lille, France). For detection, a CCD detector (Wright Instruments Ltd., Enfield, U.K.) with 1024 pixels was used. An Ar^+ ion laser operating at a wavelength of 514 nm was applied as radiation source. A laser power between 15 and 40 mW was chosen. Four different sample types were investigated in this work. The spectra of the diamond sample (abrasive wheel) show only one sharp band at 1332 cm^{-1}. The spectra of the investigated carbon nitride films are characterized by a broad band between 1000 and 1800 cm^{-1}. This peak can be described by the ratio of the intensities I_D/I_G of the so-called D (disorder) peak at 1350 cm^{-1} and the G (graphite) peak at 1580 cm^{-1}. At 520 cm^{-1}, a sharp peak was observed. This peak was assigned to the silicon substrate. That means that the radiation partly penetrates the thin (100-nm) carbon nitride films. For comparison, an untreated silicon wafer used for the preparation of carbon nitride films was also investigated. At last, a graphite electrode was measured. Its spectra are characterized by the main peak at 1580 cm^{-1}, the graphite peak.

The computations were performed on a PC using the MATLAB-package 5.2[38] and the Wavelet toolbox.[27] The intensity of the spectra was normalized to the interval 0−1. Renormalization was applied after despiking. The following wavelet bases have been applied during the current investigations. Wavelets abbreviated by Db belong to the Daubechies wavelet family; the number characterizes the number of vanishing moments. Analogously, the Coiflets are characterized by Coif and the Symlets, by Sym appended by its number of vanishing moments. The Haar wavelet is identical to Db1. Biorthogonal spline wavelets as Bior6.8 exhibit different pairs of decomposition and reconstruction wavelets and scaling functions. Estimation of σ_{level} was performed as implemented in the function wnoisest[27] (generalization of eq 3).

RESULTS AND DISCUSSION

At first, it was investigated whether the standard wavelet transform methods for denoising would perform despiking and denoising simultaneously. It should be discussed for the Raman spectrum of a carbon nitride film by means of Figure 1. The spectrum exhibits four spikes (S1−S4) and a narrow band (B1) at 520 cm^{-1}. The wavelet decomposition was performed by the Coif5 wavelet from the first to the fourth level. The juxtaposition of approximations and details enables a coherent view of low- and high-frequency components over several scales. Practically, we have applied the crudest form of wavelet denoising to see how the spikes behave at each level j of the decomposition. The

(34) Donoho, D. L. *IEEE Trans. Inf. Theory* **1995**, *41*, 613−627.
(35) Donoho, D. L.; Johnstone, I. M.; Kerkyacharian, G.; Picard, D. *J. R. Stat. Soc., Series B* **1995**, *57*, 301−337.
(36) Donoho, D. L.; Johnstone, I. M. *Biometrika* **1994**, *81* (3), 425−455.
(37) Misiti, M.; Misiti, Y.; Oppenheim, G.; Poggi, J.-M. *Wavelet Toolbox User's Guide*; The Mathworks Inc.: Natick, MA, 1997; pp 8−190.
(38) MATLAB 5.2 for Windows; The Mathworks Inc.: Natick, MA.

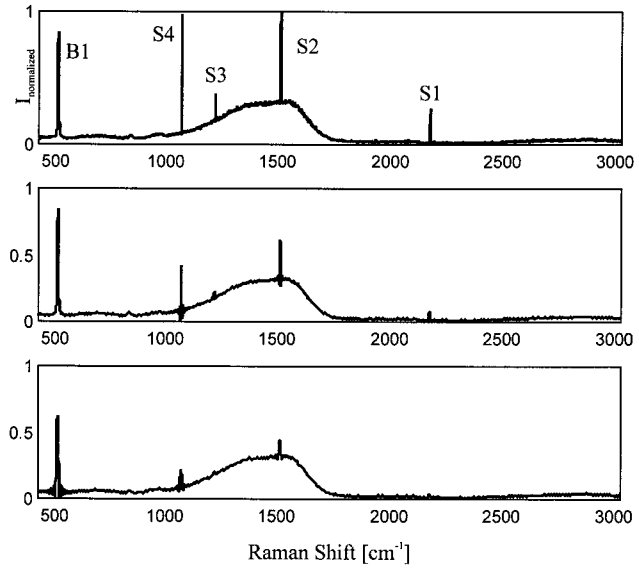

Figure 2. Fourier decomposition and reconstruction of the carbon nitride film Raman spectrum: original spectrum (top), reconstruction after setting 83% (middle), and 93% (bottom) of the coefficients to zero.

strategy would be worthy to perform more refined investigations if the approximation A_j at a distinct level j would possess the following properties: (i) the intensity of band B1 has been slightly reduced by its noisy part, (ii) the band profile has been preserved and, (iii) the spikes have disappeared at that level, j.

It becomes evident from Figure 1 that the desired behavior has not occurred. As with noise, spikes S1−S4 are represented within the details D_j; but like the band, the spikes also appear within the approximations A_j. Even at level 4, spikes are clearly perceptible; however, beginning with level 3, the band B1 has already been deformed, applying the crude denoising strategy. The tendency is for the amplitude of the spikes to diminish with larger details, D_j, but a temporary rise of some spike details may also be observed. It occurs with the double-peaked spike S2, which is no longer resolved beginning with level 3. The temporary enhancement of spike detail amplitudes may also be observed on the trapezoidally shaped spike S4 that has intensity maximums at levels 2 and 3. The band B1 steadily increases its detail coefficients from levels 1−4.

Signal deformation and simultaneous preservation of spike portions was observed for all of the wavelet bases shown in Figure 3. Consequently, we had to conclude that in general, despiking of Raman spectra could not be performed simultaneously while denoising them. Obviously, both band and spike share common frequency components, as was confirmed by Fourier analysis. The middle and bottom parts of Figure 2 show two different Fourier reconstructed spectra. The first one was reconstructed setting 83% and the second one setting 93% of the Fourier coefficients to zero. The original spectrum is shown at the top for comparison. As with the wavelet decomposition, a complete removal of spikes cannot be achieved without serious band distortion. Hence, there is no straightforward way to construct suitable filters.

In a second approach, we exploited the observation that a discrimination of spikes from bands as well as from noise occurs within the details. The best discrimination was observed by the first-level details (D_1), in accordance with the recommendation

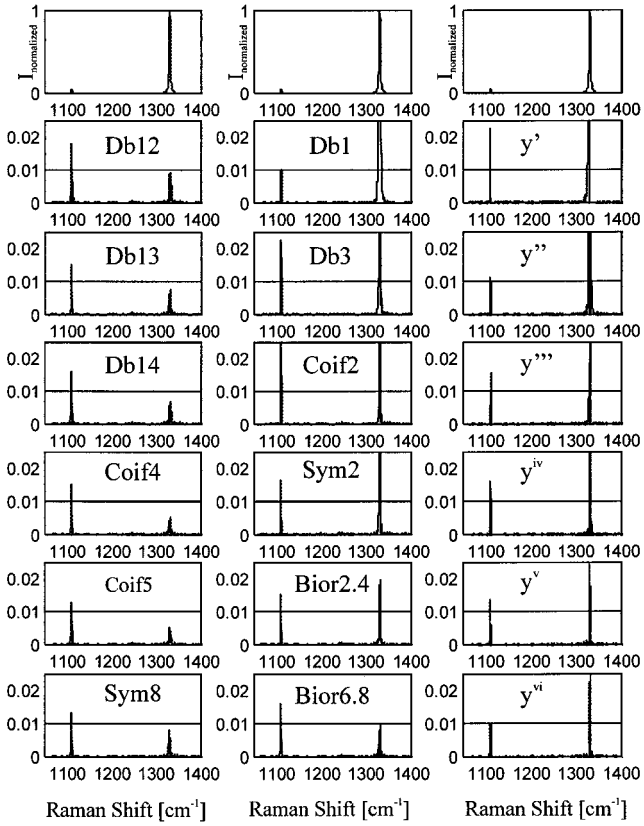

Figure 3. Wavelets for discriminating a narrow Raman band (fwhm = 3 cm^{-1}) from spikes. Suitable wavelets (left column): Raman spectrum of the diamond sample and $|D_1|$ details of Db12, Db13, Db14, Coif4, Coif5, and Sym8. Unsuitable wavelets (middle column): Raman spectrum of the diamond sample and $|D_1|$ details of Db1, Db3, Coif2, Sym2, Bior2.4, and Bior6.8. For all of the wavelets, the level 1 details are shown. Absolute values of first to sixth derivatives (right column) for comparison.

given in ref 39 The spike locations may be projected into the appropriate locations of the original spectrum; hence, after recognition and projection, spike removal could be performed in the original domain by conventional methods as interpolation or regression. It is impossible to apply this strategy to Fourier analysis, because the latter has the disadvantage of losing time information after transforming a signal into the frequency domain. In effect, the localization of spikes owing to their frequency analysis is not feasible; therefore which wavelets are suitable for spike recognition and which thresholds have to be chosen to separate spikes and bands by their D_1 coefficients was analyzed.

Selection of Suitable Wavelets. Because of the necessity of threshold selection, the risk of first or second-order mistakes resulting from the chosen threshold will always persist. Hence, the wavelet selection and appropriate threshold selection had to be adapted to the experimental conditions. Because the discrimination problem becomes more difficult with narrower bands, the narrowest bands to be expected in our experiments should be applied for the threshold selection as reference. According to our experimental design, we have to expect bands from the diamond sample series and from silicon wafers to be the narrowest bands (fwhm $\approx$ 3 cm^{-1}). To avoid misinterpreting end effects as spikes, the first three boundary points were excluded from interpretation.

(39) Misiti, M.; Misiti, Y.; Oppenheim, G.; Poggi, J.-M. *Wavelet Toolbox User's Guide*; The Mathworks Inc.: Natick, MA, 1997; pp 3−3.

Table 1. Noise Estimates for the Raman Spectrum of a Carbon Nitride Film

wavelet level	σ_{level}[a]			y_{max}/σ_{level}[b]			std(y)/σ_{level}[c]		
	1	2	3	1	2	3	1	2	3
Db12	0.0046	0.0064	0.0068	215	157	146	24	18	16
Db13	0.0046	0.0064	0.0065	217	157	153	24	18	17
Db14	0.0046	0.0065	0.0069	219	154	145	24	17	16
Coif4	0.0046	0.0064	0.0069	216	156	146	24	17	16
Coif5	0.0046	0.0064	0.0067	218	156	149	24	17	17
Sym8	0.0046	0.0063	0.0069	216	159	146	24	18	16

[a] Level-dependent estimated standard deviation of noise. [b] y, intensity of the despiked and renormalized to the range 0−1 Raman spectrum; std(y). [c] Standard deviation of intensity.

Table 2. Local Absolute Maximums of First Level Details and Derivatives without and with Preliminary Denoising the Raman Spectrum of a Carbon Nitride Film[a]

wavelet	Details $\lvert D_1\rvert_{max}$ without denoising		Details $\lvert D_1\rvert_{max}$ after denoising	
	band at 517 cm^{-1}	spike at 2180 cm^{-1}	band at 517 cm^{-1}	spike at 2180 cm^{-1}
Db12	0.017	0.11 (6.4)	0.000	0.08 (219.5)
Db13	0.016	0.11 (7.2)	0.001	0.09 (191.2)
Db14	0.013	0.10 (8.1)	0.000	0.08 (>1000)
Coif4	0.015	0.12 (7.9)	0.001	0.10 (102.3)
Coif5	0.015	0.12 (7.7)	0.001	0.10 (89.3)
Sym8	0.013	0.11 (8.6)	0.000	0.10 (>1000)
	Absolute Values of Derivatives without Denoising		Absolute Values of Derivatives after Denoising	
y'	0.103	0.13 (1.3)	0.095	0.10 (1.1)
y''	0.042	0.13 (3.1)	0.033	0.10 (3.1)
y'''	0.022	0.10 (4.4)	0.012	0.08 (6.3)
y^{iv}	0.015	0.10 (6.5)	0.005	0.07 (14.6)

[a] The ratio of spike to band value is denoted in parentheses.

For Figure 3, the Raman spectrum of a diamond sample was selected. Besides the band at 1330 cm^{-1}, a small spike with about 5% intensity in relation to the band maximum is localized at 1100 cm^{-1}. In the left column of Figure 3, the absolute values $|D_1|$ of level-1 detail coefficients were calculated as indicator functions for the wavelets Db12, Db13, Db14, Coif4, Coif5, and Sym8. The band coefficients lie below the empirically chosen threshold for despiking, $thr_s = 0.01$ and all of the spike coefficients lie above it. Compare it with the middle column of Figure 3, where indicator functions are shown relying on wavelet decompositions using Db1, Db3, Coif2, Sym2, Bior2.4, and Bior6.8 wavelets. The comparison shows that those wavelets are suitable for spike indications that exhibit a high number of vanishing moments within a wavelet family, for example, Db14, Coif5, or Sym8. Most of the unsuitable wavelets shown in the middle column of Figure 3 cause the indicator function become larger for the band, as for spikes. With respect to biorthogonal spline wavelets, we found that the best ones of them just reache the threshold (Bior6.8). For comparison, absolute values of derivatives are represented as indicator functions in the right column of Figure 3. The figure clearly shows its inferiority with respect to suitable wavelets arranged in the left column.

Influence of Noise on Spike Recognition. Next, the influence of noise and denoising on spike recognition and discrimination has been investigated. Denoising at this stage in the procedure was assumed to be a temporary operation. That means that refined denoising should be performed afterward. In Tables 1 and 2, the results from the investigation of the carbon nitride film are summarized. Table 1 shows estimates for the standard deviation of the noise and two expressions for the signal-to-noise ratio. The noise estimation was performed separately after spike removal and renormalization to the interval 0−1. Including or excluding the spike removed regions did not influence the estimations at the chosen round-off precision. The standard deviation of the noise was estimated separately for the first through third levels by the wnoisest function of the Matlab Wavelet Toolbox[27] according to eq 3. The wavelets used for decomposition are listed in Table 1. Besides the wavelet-based estimation, a conventional method was applied for noise estimation.[40] For that purpose, spectral intervals were selected that did not show absorption or drift. The conventional estimation relies on formula

$$\sigma = (\text{noise}_{max} - \text{noise}_{min})/5 \qquad (6)$$

According to eq 6, the standard deviation of the noise of the carbon nitride film Raman spectrum was estimated to be $\sigma = 0.0063$ and $\sigma = 0.0042$ for the intervals 2136−2319 cm^{-1} and 2015−2059 cm^{-1}, respectively.

The main columns of Table 1 show the standard deviation of the noise, the signal-to-noise ratio with respect to the band maximum of the largest band, and a term that characterizes overall behavior of spectral information with respect to noise. The latter equals the ratio of the standard deviation of the variables with respect to the standard deviation of the noise. Due to the chosen normalization, S/N at the band maximum equals the reciprocal of the standard deviation of the noise. Roughly, the range of noise estimated by wavelet decomposition agrees with that by classical analysis; however, the wavelet analysis reveals more information. The noise estimation by wavelet decomposition shows a tendency to enlargement from the first to the third level. Comparing with the other two levels, the analysis of level 1 details leads to a considerably smaller estimation of the noise. That gives reason to suppose nonwhite noise.

Table 2 shows the effect of preliminary denoising on the discrimination of level 1 details $|D_1|$. The spectrum is visualized in Figure 1; fwhm of the band equals 6 cm^{-1}. The spike details exhibit the same order of magnitude before and after denoising. In contrast, the peak details have been diminished by at least 1 order of magnitude. Consequently, as result of that pretreatment, the discrimination will be improved. Otherwise, erroneous band rejection had been occurred using $|D_1| = 0.01$ as threshold. Additionally, the first through fourth derivatives were calculated. As with the D_1 details, its absolute values serve as indicator function. We see the improvement of the discrimination from the first to the fourth derivative. For the noisy spectrum, the higher derivatives are almost as equally suited as the D_1 coefficients to separate that band from spikes, in contrast to the diamond sample (cf. Figure 3); however, less improvement will be obtained by

(40) Skoog, D. A.; Leary, J. J. *Principles of Instrumental Analysis*, 4th ed.; Saunders College Publishing: Orlando, FL, 1992; p 47.

Table 3. Savitzky−Golay Fourth-Order Polynomial Smoothing: First to Fourth Derivatives of the Raman Spectrum of a Carbon Nitride Film[a]

	window width (no. of points) 5		window width (no. of points) 7		window width (no. of points) 9		window width (no. of points) 15		window width (no. of points) 21	
derivative	band at 517 cm^{-1}	spike at 2180 cm^{-1}	band at 517 cm^{-1}	spike at 2180 cm^{-1}	band at 517 cm^{-1}	spike at 2180 cm^{-1}	band at 517 cm^{-1}	spike at 2180 cm^{-1}	band at 517 cm^{-1}	spike at 2180 cm^{-1}
y'	0.106	0.171 (1.6)	0.102	0.089 (0.9)	0.104	0.058 (0.6)	0.094	0.022 (0.2)	0.082	0.011 (0.1)
y''	0.044	0.236 (5.4)	0.023	0.078 (3.4)	0.018	0.037 (2.1)	0.016	0.008 (0.5)	0.013	0.003 (0.2)
y'''	0.007	0.040 (5.5)	0.003	0.010 (3.5)	0.002	0.004 (2.1)	0.001	0.001 (0.5)	0.001	0.000 (0.3)
y^{iv}	0.006	0.043 (7.6)	0.001	0.006 (5.8)	0.000	0.002 (5.0)	0.000	0.000 (1.1)	0.000	0.000 (0.4)

[a] The ratio of spike to band value is denoted in parentheses.

preliminary wavelet denoising in comparison with the D_1 details, as may be seen from the ratios of the appropriate spike-to-band values that are denoted in parentheses in the spike columns.

For comparison, a Savitzky−Golay[41] fourth-order polynomial smoothing was performed. In Table 3, the first through fourth derivatives of the Raman spectrum of a carbon nitride film are shown. Ratios of the appropriate spike-to-band values are denoted in parentheses in the spike columns, as in Table 2. The derivatives were calculated dependent on the window width, that is, the number of neighboring points used for the polynomial smoothing. A smaller window size causes less smoothing and leads to greater discrimination of bands vs spikes, as shown in Table 3. A large window size may even lead to a wrong reversal of the spike-vs-band indication, as shown for the application of 15- and 21-point-size windows. This behavior may be explained to be a result of the fact that more complete smoothing led to height reduction and broadening of signals with small fwhm, as compared with broader signals;[14,42] however, even in the most favorable case (5-point window width) Savitzky−Golay smoothing has been only slightly improved for discrimination between bands and spikes as compared with the original unprocessed data. Less improvement of the derivative ratios of that method has been achieved in comparison with those based on wavelet denoising. A large discrepancy exists with respect to the $|D_1|_{max}$ details after its denoising (cf. Tables 2 and 3).

Tables 4 and 5 show the results for the diamond sample. Visually, noise is hardly recognizable. At this high S/N, a very good agreement between conventional and wavelet-decomposition-based estimation of noise has been achieved. According to eq 6, the noise was estimated to be in the range of 0.0002−0.0003 for different spectral intervals. The estimations by the wnoisest function are summarized in Table 4. According to the expectation, denoising at this high S/N will have almost no influence on either the band or the spike details (cf. Table 5). To see how robustly the threshold behaves against perturbations, we enlarged the noise by adding artificial noise to the diamond spectrum. To be comparable with the investigations of the carbon nitride film, the standard deviation was chosen to be $\sigma = 0.005$.

Table 6 shows the effect of preliminarily denoising the artificial noise prior to spike recognition on the small spike and the band; compare to Figure 3 for visualization of the intensity ratio between spike and band. Regarding the spike, the indicator function has been diminished below the threshold value of 0.01. Really, that behavior was expected. The small spike is not well-separated from

Table 4. Noise Estimates for the Raman Spectrum of a Diamond Sample

wavelet level	σ_{level}[a]			y_{max}/σ_{level}[b]			std(y)/σ_{level}[c]		
	1	2	3	1	2	3	1	2	3
Db12	0.0002	0.0003	0.0003	5045	3660	3571	342	248	242
Db13	0.0002	0.0003	0.0003	5238	3769	3988	355	256	271
Db14	0.0002	0.0003	0.0002	5311	3768	4000	360	256	271
Coif4	0.0002	0.0002	0.0002	5198	4156	4083	353	282	277
Coif5	0.0002	0.0002	0.0002	5217	4144	4194	354	281	285
Sym8	0.0002	0.0003	0.0003	5205	3898	3898	353	264	264

[a] Level-dependent estimated standard deviation of noise. [b] y, intensity of the despiked and renormalized to the range 0−1 Raman spectrum. [c] Std(y), standard deviation of intensity.

Table 5. Local Absolute Maximums of First-Level Details without and with Preliminary Denoising the Raman Spectrum of the Diamond Sample

	details $\|D_1\|_{max}$ without denoising		details $\|D_1\|_{max}$ after denoising	
wavelet	band at 1330 cm^{-1}	spike at 1110 cm^{-1}	band at 1330 cm^{-1}	spike at 1110 cm^{-1}
Db12	0.009	0.018	0.008	0.017
Db13	0.007	0.016	0.006	0.015
Db14	0.005	0.013	0.004	0.012
Coif4	0.008	0.015	0.007	0.015
Coif5	0.005	0.015	0.004	0.015
Sym8	0.008	0.013	0.007	0.013

Table 6. Local Absolute Maximums of First-Level Details without and with Preliminary Denoising the Raman Spectrum of a Diamond Sample[a]

	details $\|D_1\|_{max}$ after denoising	
wavelet	band at 1330 cm^{-1}	spike at 1110 cm^{-1}
Db12	0.000	0.000
Db13	0.000	0.000
Db14	0.000	0.000
Coif4	0.000	0.001
Coif5	0.000	0.001
Sym8	0.000	0.001

[a] Artificial noise with $\sigma = 0.005$ was added to the spectrum.

(41) Savitzky, A.; Golay, M. J. E. *Anal. Chem.* **1964**, *36*, 1627−1639.
(42) Press, W. H.; Teukolsky, S. A.; Vetterling, W. T.; Flannery, B. P. *Numerical Recipes in C*, 2nd ed.; Cambridge University Press: New York, 1992.
(43) Ehrentreich, F. Fresenius' J. Anal. Chem., submitted for publication.

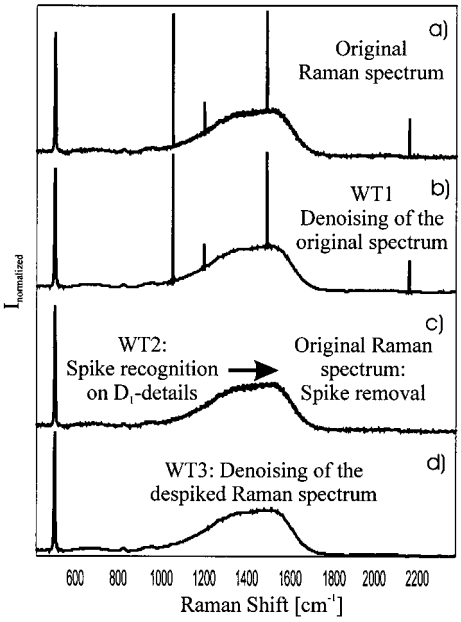

Figure 4. Main steps of the proposed procedure: (a) raw spectrum, (b) wavelet transform for preliminary denoising of the spectrum; (c) wavelet transform for spike recognition and spike removal of the original signal; and (d) wavelet transform for final denoising.

the noise, and consequently, its wavelet details coefficients d_1 have been removed together with those of the noise during preliminary denoising.

In comparison with Table 5, the size of the band detail coefficients has been further diminished. Obviously, the band has been more smoothly adapted, together with the removal of a larger noise portion. That supposition will be supported by the fact that the wavelet types should be identical for preliminary denoising and subsequent spike recognition; otherwise, the effect is not pronounced. Consequently, during the second wavelet transform, an almost perfect match between wavelet approximation and smoothed band will be obtained. As a premise, some minimal degree of band smoothness must already exist to support the discrimination. Signal shapes, like those from spikes that exhibit a triangular or trapezoidal form and differ very much from Gaussian or Lorentzian shape, do not exhibit sufficient smoothness, a useful property for the reliable discrimination between bands and spikes.

After spike recognition, the "spiky" regions will be overwritten by linearly interpolated values. Those values will be projected into the original noisy spectrum. The reason to do so is that some lack of spike approximation at its basis. Comparable to Fourier transform, side lobes appear at the bases of spikes in the course of denoising.

Figure 4 gives an overview of the main steps of the proposed procedure. The raw spectrum (a) is processed by a first wavelet transform for preliminary denoising the spectrum (b). A second wavelet transform is applied to decompose the signal into level 1 approximations and details. Recognition of spikes is performed by its level 1 details $|D_1|$ and spike removal is performed after projection to the original signal (c). A third wavelet transform is applied for final denoising (d).

The final denoising was performed by Coif5 level-5 decomposition. Because of supposed deviations from white noise, as was explained above, the selection of that level was performed empirically by visual inspection. As with the first denoising step, soft thresholding was applied. The denoising threshold thr was estimated according to Equation 5.

Two further treatments of experimental spectra are shown in Figures 5 and 6. In each case, the top panels (a) show the original spectrum, panels b show the indicator function $|D_1|$, and panels c show the processed, that is, denoised and despiked, spectrum. Additionally, the despiking threshold $thr_s = 0.01$ is indicated as a straight line. Figure 5 stems from processing a Raman spectrum of a silicon wafer that exhibits a small band and some small spikes.

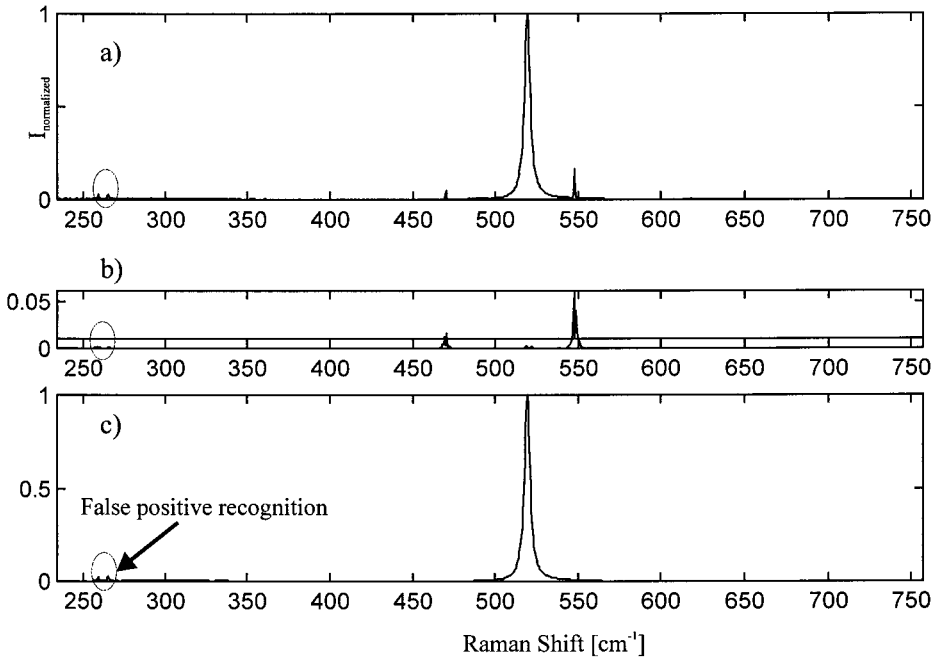

Figure 5. Complete processing of Raman spectra of a silicon wafer sample: (a) original spectrum, (b) level 1 detail coefficients, $|D_1|$, and (c) despiked and denoised spectrum.

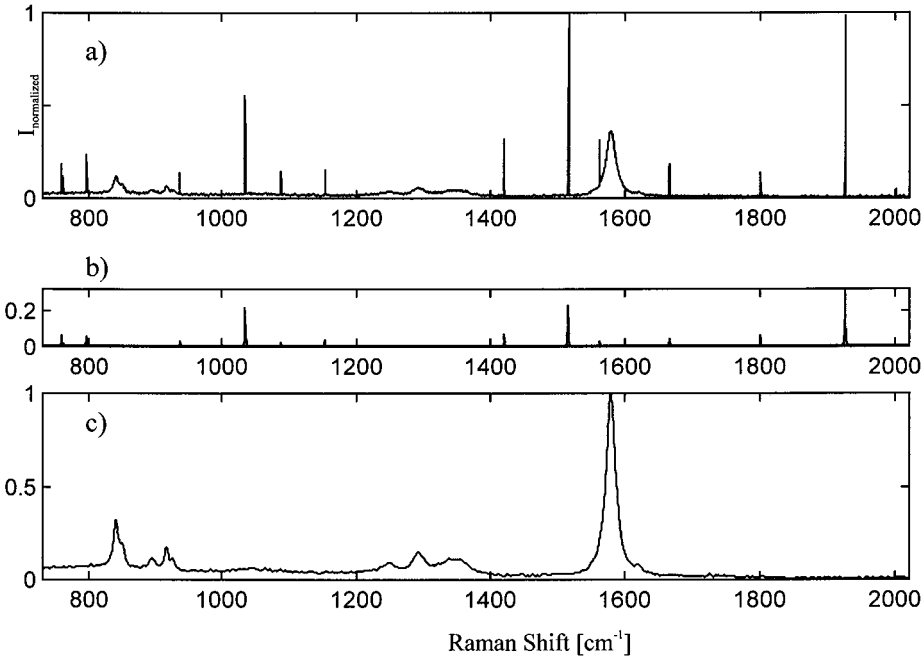

Figure 6. Complete processing of Raman spectra of a graphite sample: (a) original spectrum; (b) level 1 detail coefficients, $|D_1|$; and (c) despiked and denoised spectrum. Note the renormalization.

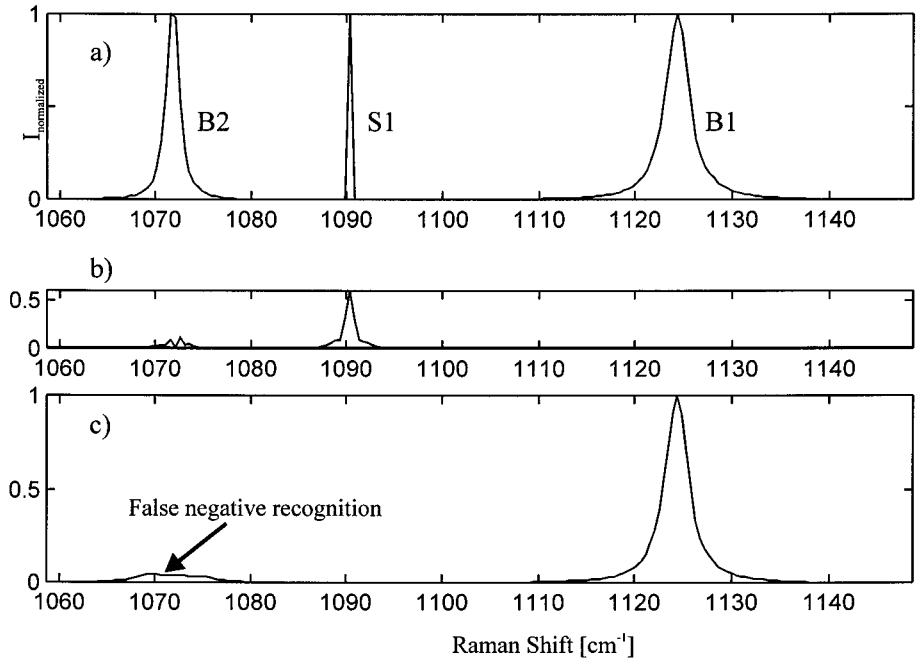

Figure 7. Erroneous band suppression in an artificial spectrum: (a) artificial spectrum consisting of band B1 (fwhm = 3 cm^{-1}) from the diamond spectrum, band B2 (fwhm = 1.5 cm^{-1}), and spike S1 (fwhm = 0.5 cm^{-1}); (b) level 1 detail coefficients, $|D_1|$; and (c) processed spectrum.

Figure 6 is due to processing the Raman spectrum of graphite that is overcrowded with spikes. Wavelet decompositions by the Coif5 wavelet were applied using $thr_s = 0.01$ as threshold for spike discrimination and $j = 5$ as level for denoising, as before.

Limitations. From the silicon wafer spectrum (cf. Figure 5), a restriction is visible that concerns very tiny spikes. In some instances, they cannot be reliably differentiated from the bands leading to a false-positive recognition by a pure wavelet-based approach; however, such tiny spikes are easily removed due to their small differences from the baseline.

Two further restrictions on extreme case studies will be explained. Those simulations rely on a small library of typical spikes, peaks, and model band profiles. To see the limitations, even if not to be expected in our practice, or at least not shown within our real Raman spectra, simulations were performed.

In Figure 7, as an example of a false negative error, a simulated spectrum is shown that consists of the real diamond band B1 (fwhm = 3 cm^{-1}), the simulated diamond band B2 (fwhm = 1.5 cm^{-1}), and a spike S1 (fwhm = 0.5 cm^{-1}). All of the signals exhibit an identical intensity maximum. It may be seen that the coef-

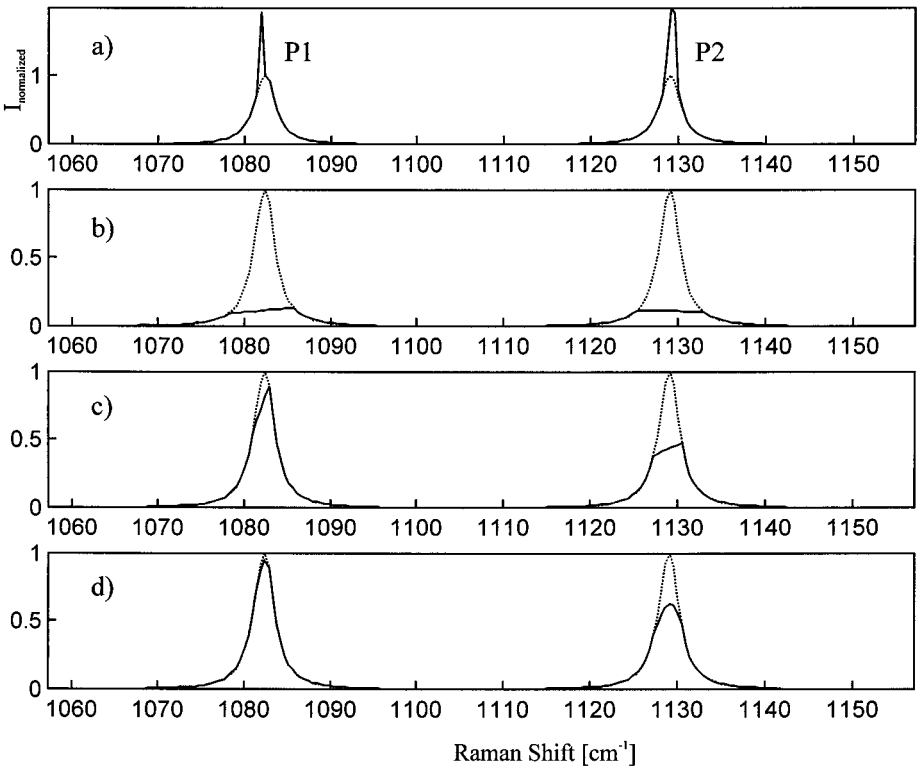

Figure 8. Processing of artificial band patterns. (a) Pattern P1 consists of the superposition of a triangular spike on the peak of a band. For pattern P2, a trapezoidal spike was used. (b) Reconstructions are shown for despiking based on threshold $thr_s = 0.01$; (c) $thr_s = 0.1$, linear interpolation;and (d) $thr_s = 0.1$, cubic interpolation. The undisturbed band is drawn as a dotted line for comparison.

ficients of band B2, in contrast to the real band B1, exceed the threshold of $thr_s = 0.01$ considerably. Correctly, its amplitude is smaller than the amplitude of spike S1. By adjusting the threshold to a value $thr_s = 0.15$ after visual inspection that is clearly superior in comparison with the algorithm, spike S1 and band B2 will be separated correctly. Note that the shape of band B2 above fwhm is described only by three points, whereas band B2 is described by 6 points.

A second important point considers the superposition of spikes with bands. Obviously, no problem arises with broad bands, as may be seen from the spiky graphite spectrum (Figure 6). As a worst case, we can imagine that spikes are overlaid on top of the band, as shown in Figure 8. The reference bands B1 and B2 are identical (fwhm = 3 cm^{-1}), but the spike shapes differ. Band B1 is overlaid by a triangular spike (fwhm = 0.5 cm^{-1}), and band B2 is overlaid by a trapezoidal one (fwhm = 1 cm^{-1}). For comparison, the undisturbed band is drawn in Figure 8b−d as dotted line. The useless reconstruction shown in Figure 8b relies on a threshold of 0.01; those in Figure 8c,d rely on a threshold of 0.1. Their differences consist of the selection of interpolation functions. For the former rough reconstruction, a linear interpolation, and for the latter, a cubic one was used.

Fortunately, the probability that difficult-to-resolve superpositions occur is not large; however, if superpositions are obtained, the analyst should balance the effort of individual adaptation strategies vs a repetition of the experiment.

CONCLUSION

Suppression of spikes is not straightforward, possibly by the wavelet transform; however, the despiking and denoising of Raman spectra could be performed sequentially by multiple wavelet decompositions of the spectrum. Despiking as a partial step of the procedure could be managed by replacing the generally accepted decomposition/processing/reconstruction strategy. The sequential analysis requires applying the wavelet transform in repetitive mode for (i) preliminary denoising, (ii) despiking, and (iii) refined denoising. The procedure has advantageously used the dual localization property of wavelets, enabling projection of spectral features from one representation to another; hence, feature recognition and processing could be performed by its most suitable representation in the appropriate space.

Wavelets having a low number of vanishing moments were not suitable for spike indication of Raman spectra. Wavelet bases from the Daubechies, Symlet, and Coiflet families with high number of vanishing moments could be derived as suitable wavelets for the despiking of Raman spectra.

As with other low-dimensional feature recognition problems, the naked eye is the more adaptive pattern recognizer, provided that the resolution of the features is sufficient. In Figure 7, by visual inspection one would only remove S1 but certainly not B2. In contrast, in Figure 1 without zooming band B1 interactively, discrimination from spikes is hardly possible.

Due to the necessity of threshold selection, the risk of first- or second-order mistakes depending on the chosen threshold will always persist. Because false negative errors are more serious, the threshold should be chosen in a way to avoid removal of bands. Hence, the threshold selection had to be adapted to the experimental conditions. Limitations are due to the ratio of bandwidth to resolution; as a rule of thumb and because of

complex superpositions between bands and spikes, the band shape should be described by at least 6 points above its half-height. Improvement of difficult instances might be performed by individual adaptation, including wavelet packet transform;[43] however in extreme cases, a higher experimental expenditure is inevitable. A duplication of the measurement, if possible, would make the identification of cosmic peaks straightforward, because they would show up at different wavelengths, thus exploiting the fact that spikes are distributed randomly over the CCD chip.

ACKNOWLEDGMENT

The work was funded by the "Deutsche Forschungsgemeinschaft" (Eh 121/2-1).

Received for review November 27, 2000. Accepted May 16, 2001.

AC0013756